CORE
Metadata, citation and similar papers at core.ac.uk
Provided by Elsevier - Publisher Connector


Available online at www.sciencedirect.com
ScienceDirect
Procedia IUTAM 19 (2016) 136 – 143
Procedia IUTAM
www.elsevier.com/locate/procedia

IUTAM Symposium Analytical Methods in Nonlinear Dynamics

Heave-imposed motion in vertical risers: a reduced-order modelling based on Bessel-like modes

Carlos E.N. Mazzilli[a]*, Fabio Rizza[b], Thiago Dias[a]

[a]*Escola Politécnica, University of São Paulo, Av. Professor Luciano Gualberto, Trav 3 no. 380, 05508-010 São Paulo, Brazil*
[b]*Politecnico di Milano, Piazza Leonardo da Vinci, 32, 20133 Milano, Italy*

Abstract

The heave-imposed excitation in vertical risers is a problem of scientific and technological interest, since it can lead to parametric instabilities on one hand, and fatigue failure with disastrous environmental and financial consequences on the other. The paper addresses a reduced-order analytical model of risers using Bessel-like modes as projecting functions and compares its dynamical response to experimental results from a towing tank test.

© 2016 The Authors. Published by Elsevier B.V. This is an open access article under the CC BY-NC-ND license (http://creativecommons.org/licenses/by-nc-nd/4.0/).
Peer-review under responsibility of organizing committee of IUTAM Symposium Analytical Methods in Nonlinear Dynamics
Keywords: marine riser; reduced-order model; Bessel-like mode; Mathieu's instability; heave-imposed motion

1. Introduction

Recent discoveries of oil and gas fields, some hundred kilometres off the Brazilian Southeast coast, in ultra-deep waters, demand scientific and technological advances towards their safe and economic exploitation. Among the challenges posed to scientists and engineers, the dynamic analysis of offshore risers is of primary relevance, due to fatigue of the structural material. This is specially the case of risers subjected to heave-imposed motions.

Heave motions of floating unities, due to gravity surface wave action, may cause transversal vibrations in vertical risers. In fact, heave imposes tension amplitude modulation to the long and flexible tubular structure, which may drive parametric resonance as a consequence of the well-known Mathieu's instability[1]. Chatjiorgeorgiou and Mavrakos[2] address the classic monochromatic excitation case, whereas Yang et al[3] and Lei et al[4] consider multi-frequency excitations. The analysis of the riser dynamic response is here tentatively addressed by reduced-order models of a pre-

* Corresponding author. Tel.: +55-11-3091-5232; fax: +55-11-3091-5681.
E-mail address: cenmazzi@usp.br

2210-9838 © 2016 The Authors. Published by Elsevier B.V. This is an open access article under the CC BY-NC-ND license (http://creativecommons.org/licenses/by-nc-nd/4.0/).
Peer-review under responsibility of organizing committee of IUTAM Symposium Analytical Methods in Nonlinear Dynamics
doi:10.1016/j.piutam.2016.03.018

stressed Euler-Bernoulli beam with a time-varying normal force. The dynamic problem is worked out through a standard Galerkin projection onto Bessel-like modes, as proposed by Mazzilli et al[5].

2. Continuous model

A vertical riser with length ℓ, external diameter D, cross-section area A and moment of inertia I, mass per unit length m and Young's modulus E is immersed in still water with density ρ_w . The boundary conditions at the riser top and bottom ends are indicated in two different scenarios. Firstly, for the free vibration analysis (and determination of Bessel-like modes), the pre-stressing force at the top N_t – where $N_t=N_b + p\ell$ and N_b is the bottom-end normal force – is applied by means of an imposed displacement u_ℓ at the upper support. The displacement at the top will remain constant during the free-vibration analysis, which means that the upper support will be fixed and $u(\ell,t)=u(\ell,0)$ – see Fig. 1 (a). For the second scenario, that is, the forced vibration analysis, a harmonic heave-imposed motion, positive upwards, is applied at the riser top ($x=\ell$), which means that a heave motion $h(t) = h_0 cos\hat{\Omega}t$ will be superimposed to the pre-stressed equilibrium configuration – see Fig 1 (b).

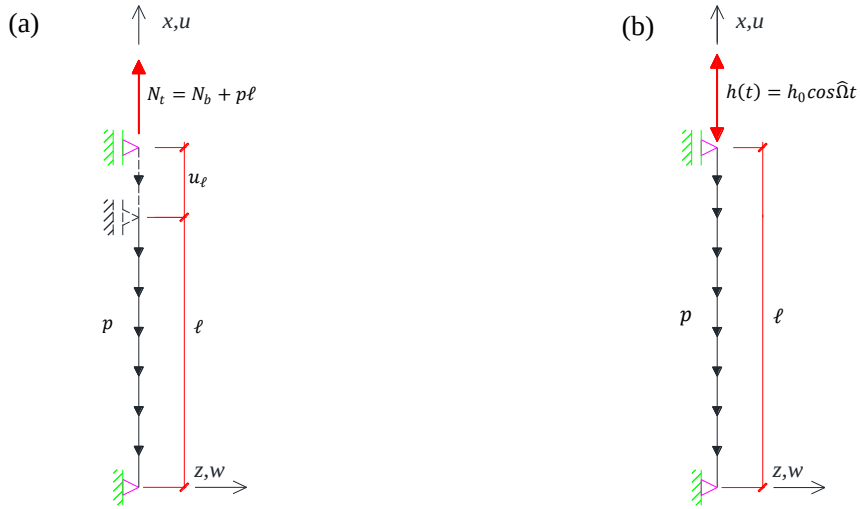

Fig. 1. (a) First scenario for the riser model; (b) Second scenario for the riser model

The mathematical model for the riser transversal motion $w(x,t)$ according to the Euler-Bernoulli beam theory, is characterised by the equation

$$m\frac{\partial^2 w}{\partial t^2} + EI\frac{\partial^4 w}{\partial x^4} - \frac{\partial}{\partial x}\left[N(x,t)\frac{\partial w}{\partial x}\right] = q_w(x,t)\,. \tag{1}$$

In (1), $N(x,t)$ is the normal force, taking into account the initially-imposed thrust at the top $N_t(0) = N(0,0)$, the immersed weight p, the heave-imposed motion $h(t)$ and the axis non-linear stretching due to bending

$$N(x,t) = N_t(0) - px + \frac{EAh(t)}{\ell} + \frac{EA}{2\ell}\int_0^\ell \left(\frac{\partial w}{\partial x}\right)^2 dx\ ; \tag{2}$$

in (1), $q_w(x,t)$ stands for the force exerted by the water on the riser per unit length, assumed to be of the Morison type[7]

$$q_w(x,t) = -C_a\rho_w\frac{\pi D^2}{4}\frac{\partial^2 w}{\partial t^2} - \frac{1}{2}C_d\rho_w D\left|\frac{\partial w}{\partial t}\right|\frac{\partial w}{\partial t}\,, \tag{3}$$

where C_a and C_d are, respectively, the added-mass and drag coefficients. Equation (1) is conveniently re-written as

$$\frac{\partial^2 w}{\partial t^2} + \alpha \frac{\partial^4 w}{\partial x^4} - [\beta + \beta_h(t)] \frac{\partial^2 w}{\partial x^2} - \gamma \left(\frac{\ell}{2} - x\right) \frac{\partial^2 w}{\partial x^2} + \gamma \frac{\partial w}{\partial x} - \mu \frac{\partial^2 w}{\partial x^2} \int_0^\ell \left(\frac{\partial w}{\partial x}\right)^2 dx = \vartheta_w(t) \,, \tag{4}$$

in which the notation

$$\alpha = \frac{EI}{m};\ \beta = \frac{\bar{N}}{m};\ \beta_h(t) = \frac{EAh(t)}{m\ell};\ \gamma = \frac{p}{m};\ \mu = \frac{EA}{2m\ell};\ \vartheta_w(x,t) = \frac{q_w(x,t)}{m}, \tag{5}$$

was introduced and $\bar{N}$ denotes the average normal force along the riser before the heave-imposed motion starts

$$\bar{N} = N_t(0) - \frac{p\ell}{2}. \tag{6}$$

Normalisation is now introduced in (4) by means of the following variables

$$v = \frac{w}{D};\ \xi = \frac{x}{\ell};\ \tau = \hat{\omega}_1 t \,. \tag{7}$$

Notice that the time was normalised with respect to the riser first-mode frequency in still water $\hat{\omega}_1$

$$\begin{gathered}
\hat{\omega}_1 = \frac{\omega_1}{\sqrt{1 + C_a^*}};\ \omega_1 = \frac{\pi}{2\ell\sqrt{m}}\left(\sqrt{N_{bn}} + \sqrt{N_{tn}}\right);\ C_a^* = \frac{\frac{\pi D^2}{4}\rho_w}{m} C_a \,; \\
N_{bn} = N_b(0) + \left(\frac{n\pi}{\ell}\right)^2 EI\left(1 + \frac{3}{16}{\eta_n}^2\right)^2 \,;\ N_{tn} = N_t(0) + \left(\frac{n\pi}{\ell}\right)^2 EI\left(1 + \frac{3}{16}{\eta_n}^2\right)^2 \,; \\
N_b(0) = \bar{N} - \frac{p\ell}{2} \,;\ N_t(0) = \bar{N} + \frac{p\ell}{2} \,;\ \eta_n = \frac{W_{on}}{r};\ r = \sqrt{\frac{I}{A}} \,,
\end{gathered} \tag{8}$$

ω_1 being the first-mode frequency in air and C_a^* conveniently defined in terms of the added-mass coefficient. W_{0n} stands for the dimensional modal amplitude (defined, for convenience, at a section where the linear-theory sinusoidal mode has a maximum) and r is the gyration radius of the riser cross section. Therefore, η_n is the non-dimensional modal amplitude, defined in terms of the gyration radius. In (8) N_{bn} and N_{tn} play the role of equivalent "cable" normal forces at the bottom and the top ends, so that the fourth-order differential equation (1) can be written as a formally identical cable second-order differential equation, for which the solution can be written in terms of Bessel functions. Details can be found in Mazzilli et al[5], but are not shown here for brevity. It should be noticed the non-linear amplitude effect given by η_n in the bending term correction of N_{bn} and N_{tn}. Also, $N_b(0)$ and $N_t(0)$, already introduced with respect to Fig. 1, are here equivalently rewritten in a more suitable form, in terms of the average static normal force $\bar{N}$.

The non-dimensional equation of motion for the continuous system becomes

$$\begin{aligned}
\frac{\partial^2 v}{\partial \tau^2} + \alpha_1 \left|\frac{\partial v}{\partial \tau}\right| \frac{\partial v}{\partial \tau} + \alpha_2 \frac{\partial^4 v}{\partial \xi^4} - \left[\alpha_3 + \alpha_h cos\left(\frac{\hat{\Omega}}{\hat{\omega}_1}\tau\right)\right] \frac{\partial^2 v}{\partial \xi^2} - \alpha_4 \left(\frac{1}{2} - \xi\right) \frac{\partial^2 v}{\partial \xi^2} + \alpha_5 \frac{\partial v}{\partial \xi} \\
- \alpha_6 \frac{\partial^2 v}{\partial \xi^2} \int_0^1 \left(\frac{\partial v}{\partial \xi}\right)^2 d\xi = 0 \,,
\end{aligned} \tag{9}$$

where

$$\alpha_1 = \frac{C_d \rho_w D r}{2m(1+C_a^*)};\ \alpha_2 = \frac{\alpha}{\widehat{\omega}_1{}^2 \ell^4 (1+C_a^*)};\ \alpha_3 = \frac{\beta}{\widehat{\omega}_1{}^2 \ell^2 (1+C_a^*)};$$
$$\alpha_h = \frac{EAh_0}{m\widehat{\omega}_1{}^2 \ell^3 (1+C_a^*)};\ \alpha_4 = \alpha_5 = \frac{\gamma}{\widehat{\omega}_1{}^2 \ell (1+C_a^*)};\ \alpha_6 = \frac{\mu r^2}{\widehat{\omega}_1{}^2 \ell^3 (1+C_a^*)}. \tag{10}$$

3. Reduced-order models

Reduced-order models can be obtained via Galerkin projection onto Bessel-like modes – see Mazzilli et al[5], according to whom the expression for the n^{th}-mode is

$$\psi_n(\xi,\eta_n) = (1+a\ell\xi)^{-\frac{1}{4}} \cdot sin\left[b\left(\sqrt{1+a\ell\xi}-1\right)\right], \tag{11}$$

where

$$a = \frac{p}{N_{bn}};\ b = \frac{n\pi}{\sqrt{1+a\ell}-1}. \tag{12}$$

Functions $\psi_n(\xi,\eta_n)$ in (11) depend on η_n because they depend on *a* and *b*, which from (12) depend on N_{bn}, which depends on η_n, by virtue of (8). A normalisation of the modal functions (11) is introduced as

$$\phi_n(\xi,\eta_n) = \frac{\psi_n(\xi,\eta_n)}{\psi_n\left(\overline{\xi},\eta_n\right)}, \tag{13}$$

so that they assume the unit value at the section $\overline{\xi}$ where the corresponding linear-theory sinusoidal mode is maximal, that is $sin\left(n\pi\overline{\xi}\right)=1$ and, therefore, $\overline{\xi}=(2n)^{-1}$. Of course, the actual maximum value of the Bessel-like mode $\psi_n\left(\tilde{\xi},\eta\right)$ occurs at a section $\tilde{\xi}\neq\bar{\xi}$ and is larger than $\psi_n\left(\bar{\xi},\eta\right)$. Hence, the function $\phi_n(\xi,\eta_n)$ assumes a maximum value that is larger than 1 at $\tilde{\xi}$. Thus, the modal displacements normalised with respect to the riser diameter *D* (which in fact correspond to v, if the response is purely in mode *n*) are

$$v_n(\xi,\eta_n,\tau) = \eta_n(\tau)\frac{r}{D}\phi_n(\xi,\eta_n). \tag{14}$$

A single-mode projection was used to address the case of the first mode (*n*=1) under parametric excitation, due to its dominating character in the response, when the forcing frequency $\widehat{\Omega}$ is twice the first-mode frequency in still water $\widehat{\omega}_1$. This is the principal Mathieu's instability scenario, for which the trivial solution is unstable and, yet, a stable non-linear periodic steady-state is seen to exist, due to the joint effect of dissipation provided by the Morison damping and the stiffness non-linearity. For the response in the first mode, the non-linear influence of η_1 on N_{b1} can be neglected. In fact, in Mazzilli et al[5] both calculations have been made, namely neglecting and not neglecting the influence of η_1 on N_{b1}, and the results were basically the same. Yet, it was also shown that this influence could not be ignored in upper modes, such as the tenth one. Therefore, it is reasonable to assume

$$N_{b1} = N_b(0) + \left(\frac{\pi}{\ell}\right)^2 EI. \tag{15}$$

The Galerkin projection leads to the reduced-order model (ROM) for this problem, according to (16). Notation was simplified, so that $\eta_1=\eta$ and over dots indicate differentiation with respect to τ. Hence, the ROM non-linear oscillator finally reads

$$\ddot{\eta} I_0 + \dot{\eta}|\dot{\eta}|\alpha_1 I_1 + \eta\left\{\alpha_2 I_2 - \left[\alpha_3 + \alpha_h \cos\left(\frac{\hat{\Omega}}{\hat{\omega}_1}\tau\right)\right] I_3 - \alpha_4 I_4 + \alpha_5 I_5\right\} - \eta^3 \alpha_6 I_6 = 0\,, \tag{16}$$

where

$$I_0 = \int_0^1 \phi^2 d\xi\,;\; I_1 = \int_0^1 |\phi|\phi^2 d\xi\,;\; I_2 = \int_0^1 \phi^{IV}\phi\, d\xi; I_3 = \int_0^1 \phi^{II}\phi\, d\xi\,;$$
$$I_4 = \int_0^1 \left(\frac{1}{2} - \xi\right)\phi^{II}\phi\, d\xi;\; I_5 = \int_0^1 \phi^{I}\phi\, d\xi;\; I_6 = \int_0^1 \phi^{II}\phi d\xi \left(\int_0^1 (\phi^{I})^2 d\xi\right). \tag{17}$$

4. Numerical simulation

A numerical simulation was carried out, by integration of equation (16), using the Dormand–Prince method (RKDP), which is a member of the Runge-Kutta ordinary-differential-equation-solver family and is implemented in the MATLAB® function ODE45. Numerical results can be compared with experimental ones obtained in LIFE&MO[6] in a towing tank facility, provided the same system parameters are used (see Table 1).

The coefficient C_a^* was calibrated by imposing the first-natural frequency in still water to be $0.84Hz$ (obtained through impact tests). Assuming a constant-tension model with tension equal to the average normal force $\bar{N}$, one obtains $C_a^* = 0.3252$, which corresponds to $C_a = 0.9998$. As for the Morison drag coefficient, it was used $C_d = 1.97$.

Non-deformed length	ℓ	2.552m	Fluid density	ρ_w	1000kgm^{-3}
External diameter	D	22.2mm	Mass ratio	C_a^*	0.3252
Gyration radius	r	6.8mm	Added mass coefficient	C_a	0.9998
Riser mass per unit length	m	1.190kgm^{-1}	Drag coefficient	C_d	1.97
Immersed weight per unit length	p	7.869Nm^{-1}	Natural frequency in air	ω_1	5.773rads^{-1}
Axial stiffness	EA	1207N	Natural frequency in still water	$\hat{\omega}_1$	5.015rads^{-1}
Bending stiffness	EI	0.056Nm²	Heave amplitude	h_0	0.025m
Average normal force	$\bar{N}$	23.65N	Heave frequency	$\hat{\Omega}$	10.030rads^{-1}

Table 1. System parameters

5. Results

Experimental tests were carried out with a pre-stressed flexible pipe (filled with stainless steel microspheres to achieve the desired mass per unit length) fixed at the bottom end, immersed in water and subjected to support excitation at its top end. The most important mechanical and fluid-dynamical similarity conditions have been respected. A system of underwater cameras was used to monitor the model motion. The experimental set-up was mounted on a frame that could run along a towing tank. In this way, besides the support-excitation at the top, also vortex-induced-vibration tests could be carried out, at the same time or not. For the purposes of the present paper, only the dynamic response due to support excitation will be addressed, in a scenario of parametric instability with respect to the first mode. The results, as obtained from the experimental tests[6] for the data of Table 1, are summarised in Figs. 2-4, for the mid-span amplitude.

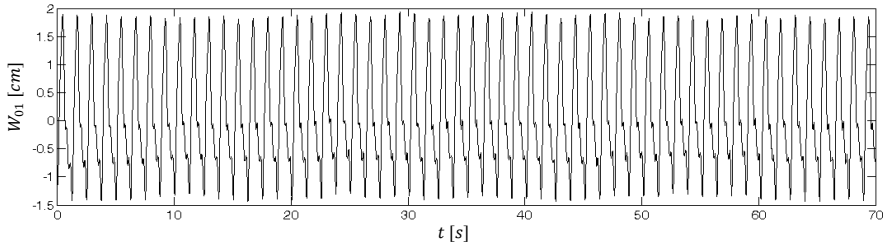

Fig. 2. Response time series for mid-span amplitude

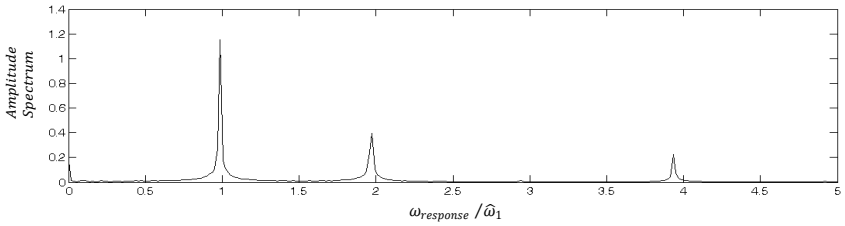

Fig. 3. Amplitude spectrum for mid-span amplitude

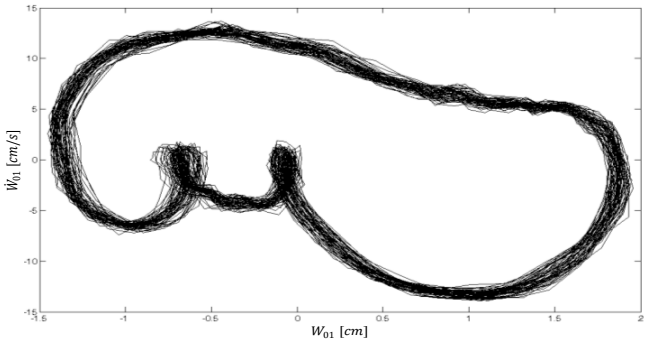

Fig. 4. Phase-plane projection for mid-span amplitude and velocity

The dynamic response, as obtained from numerical integration of equation (16) for the data of Table 1, is summarised in Figs. 5-8. Fig. 5 displays the time-response of the mid-span amplitude normalised with respect to the gyration radius.

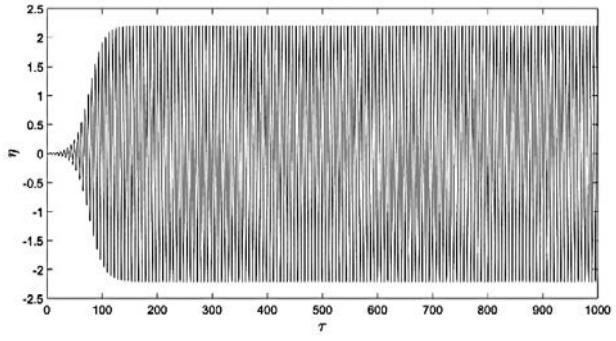

Fig. 5. Response time series for parametric resonance caused by heave motions

The non-dimensional amplitude observed was $\eta = 2.2108$. Recalling that the dimensional amplitude is obtained by multiplication by the gyration radius $r = 0.0068m$, the mid-span amplitude is found to be $W_{01} = 0.0151m$, which agrees with the experimental value[6]. Fig. 6 is a projection of the response onto the phase plane $(\eta, \dot{\eta})$, whereas Fig. 7 is the dimensional amplitude spectrum. Note that in the ROM there is a small content of the third harmonic, due to both the Bessel-like mode and the cubic non-linearity in equation (16), whereas in the experimental model there is an important contribution of the second and a minor one from the fourth harmonic, as seen in the spectrum of Fig. 3.

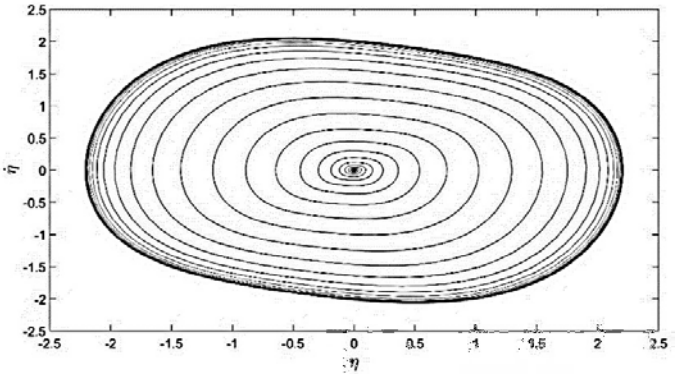

Fig. 6. Phase-plane projection for parametric resonance caused by heave motions

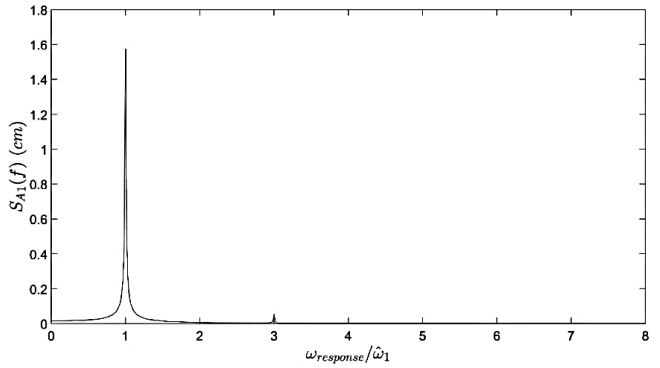

Fig. 7. Amplitude spectrum for parametric resonance caused by heave motions

It is readily noticeable that the experimental phase-space projection of Fig. 4 displays a more complex topological structure, with two "loops", as compared to Fig. 6. It is believed that the origin of the discrepancies found between experimental and reduced-order models arise from the simpler 2D modelling of the latter against the inevitable 3D character of the former. The shortcomings of the 2D model are such that, in spite of the consideration of the quadratic non-linear Morison damping, it was not capable of explaining the second harmonic contribution detected in the experimental tests (see Fig. 3). The mathematical-model response was by large dominated by the cubic non-linearity. Typical Lissajous figures were observed in the experimental tests[6] for the projected motion on the horizontal plane, with the dominating motion having half the frequency of the motion orthogonal to it. Therefore, it is reckoned that a quadratic nonlinearity associated to the coupling between the dominating and the orthogonal motions should be introduced in the model. Yet, this can only be made if a 3D mathematical modelling is pursued from the very beginning, which is beyond the scope of the present paper. Nevertheless, it should be emphasised that there is a good qualitative and quantitative correlation between the dominating planar motions, as found in the ROM using the 2D modelling and the experimental tests. Fig. 8 is a response-amplitude mapping (according to a chromatic scale) in the control-parameter plane $\left(\widehat{\Omega}/\widehat{\omega}_1, h_0\right)$, which recalls the classic Strutt's diagram (for linear systems). Yet, Fig. 8 provides information on the post-critical steady states in a region where Strutt's diagram would only foresee that the trivial solution is unstable and the response amplitude would grow without bound. This is not seen to be the case when

non-linear stiffness and Morison damping are taken into account. Mappings like this have previously been proposed by Sakamoto, in Prado et al[8], and Franzini, in Franzini et al[9], so that they are here referred to as Franzini-Sakamoto's diagrams. Observe that a narrow fringe near $\widehat{\Omega} \cong \widehat{\omega}_1$ (secondary parametric excitation) also appears, with much lower amplitudes than those observed in the primary Mathieu instability zone. One also notes the onset of the third region of instability near $\widehat{\Omega} \cong 0.67\ \widehat{\omega}_1$.

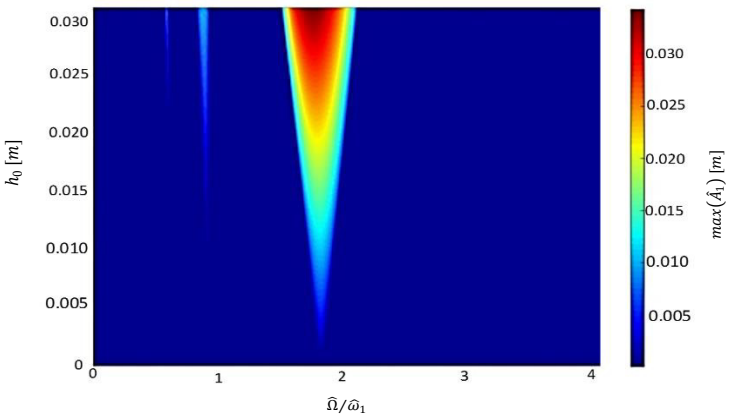

Fig.8. Franzini-Sakamoto's diagram for post-critical stable steady-state amplitudes

6. Final remarks

The reduced-order model of a riser obtained via the Galerkin method with a Bessel-like mode was capable of successfully describing both qualitatively and quantitatively the dominating behaviour of a physical model tested in a towing tank[6] in a very demanding scenario such as the Mathieu's instability caused by heave motions, as far as only planar motions are taken into account. An improvement in the reduced-order model would require a full 3D modelling, which was beyond the scope of the present paper, but will be considered in a future work.

Acknowledgements

The first author acknowledges the support of CNPq (Brazilian Science Research Council), under Grant 302757/2013-9. The authors thank Guilherme Franzini for his help in plotting Franzini-Sakamoto's diagram.

References

1. Nayfeh AH, Balachandran B. *Applied nonlinear dynamics: analytical, computational, and experimental methods*. Wiley; 2004.
2. Chatjigeorgiou IK, Mavrakos SA. Bounded and unbounded coupled transverse response of parametric excited vertical marine risers and tensioned cable legs for marine applications. *Applied Ocean Research* 2002; **24**:341–354.
3. Yang H, Xiao F, Xu P. Parametric instability prediction in a top-tensioned riser in irregular waves. *Ocean Engineering* 2013;**70**:39–50.
4. Lei S, Zhang W-S, Lin J-H, Yue Q-J, Kennedy D, Williams FW. Frequency domain response of a parametrically excited riser under random wave forces. *Journal of Sound and Vibration* 2014; **333**:485–498.
5. Mazzilli CEN, Lenci S, Demeio L. Non-linear free vibrations of tensioned vertical risers. *8th European Nonlinear Dynamics Conference*, ISBN 978-3-200-03433-4; Vienna 2014.
6. Laboratório de Interação Fluido-Estrutura e Mecânica Offshore (LIFE & MO). Hydroelastic Experiments with vertical flexible cylinders in the IPT towing tank (in Portuguese). *Technical Report RT-3; Part 4, Project "Nonlinear Dynamics of Risers" (sponsored by PETROBRAS)* 2013, 86 p.
7. Faltinsen OM. *Sea loads on ships and offshore structures*.1th ed. Cambridge: Cambridge University Press; 1990
8. Prado FS, Sakamoto FY, Mazzilli CEN. An analysis of parametric instability of risers. *Latin-American Journal of Solids and Structures* 2013; 11: 348-368.
9. Franzini GR, Mazzilli CEN. Non-linear reduced-order model for parametric excitation of vertical and immersed slender beam. International Journal of Non-Linear Mechanics 2015 (accepted for publication).